Nanomechanical coupling enables detection and imaging of 5 nm superparamagnetic particles in liquid

2011 Nanotechnology 22 125708

(http://iopscience.iop.org/0957-4484/22/12/125708)

Nanotechnology **22** (2011) 125708 (8pp) doi:10.1088/0957-4484/22/12/125708

Nanomechanical coupling enables detection and imaging of 5 nm superparamagnetic particles in liquid

Christian Dietz, Elena T Herruzo, Jose R Lozano and Ricardo Garcia

Instituto de Microelectrónica de Madrid, CSIC, Isaac Newton 8, E-28760 Tres Cantos, Madrid, Spain

E-mail: ricardo.garcia@imm.cnm.csic.es

Received 18 November 2010, in final form 16 January 2011
Published 17 February 2011
Online at stacks.iop.org/Nano/22/125708

Abstract
We demonstrate that a force microscope operated in a bimodal mode enables the imaging and detection of superparamagnetic particles down to 5 nm. The bimodal method exploits the nanomechanical coupling of the excited modes to enhance the sensitivity of the higher mode to detect changes in material properties. The coupling requires the presence of nonlinear forces. Remarkably, bimodal operation enables us to identify changes of slowly varying forces (quasi-linear) in the presence of a stronger nonlinear force. Thus, unambiguous identification of single apoferritin (non-magnetic) and ferritin (magnetic) molecules in air and liquid is accomplished.

S Online supplementary data available from stacks.iop.org/Nano/22/125708/mmedia

(Some figures in this article are in colour only in the electronic version)

1. Introduction

To analyze and understand the performance of complex materials and devices made up of nanostructures of different mechanical, electric and/or magnetic properties [1–4] requires the development of non-invasive, high resolution and single-pass characterization methods [5–11]. Recently, several multifrequency atomic force microscopy (AFM) schemes have been proposed to address the above issue [12–25]. Generically, those schemes exploit the nonlinear character of the tip–surface forces to either activate or detect higher eigenmodes or harmonics and to open new channels to improve imaging and composition sensitivity. In any force microscope the spatial resolution is ultimately controlled by the tip size and the length scale of the interaction range while the sensitivity is controlled by the thermal noise of the instrument. However, in practice the resolution and the sensitivity are controlled by two other factors, the tip–surface distance and the feedback mechanism.

To separate long-range magnetic from short-range mechanical forces a two-pass technique is applied to measure magnetic samples. In the first pass, the topography is detected while in the second pass the tip is retracted several nanometers from the imaging mode and the magnetic force is measured (lift mode). Unfortunately, the use of the lift mode decreases the lateral resolution by a factor comparable to the average tip separation (lift distance). In addition, the feedback mechanism in the conventional single (monomodal) excitation/detection regime inhibits the use of the phase shift to detect several interactions. Thus, it limits the resolution and the sensitivity of the instrument when other interactions, for example non-mechanical forces, are present. A central problem in force microscopy is how to improve the spatial resolution and the sensitivity of the instrument at a fixed thermal noise background.

Nanoscale magnetic domains have a central role in several biological and synthetic systems [26–29]. Magnetic nanoparticles are also being used as agents for cancer treatment [26] or can be used to stimulate different cell functions [27, 28]. Similarly, very small magnetic nanoparticles with a high anisotropy could be used for high-density data storage media [30]. Those applications require the simultaneous imaging, detection and eventually

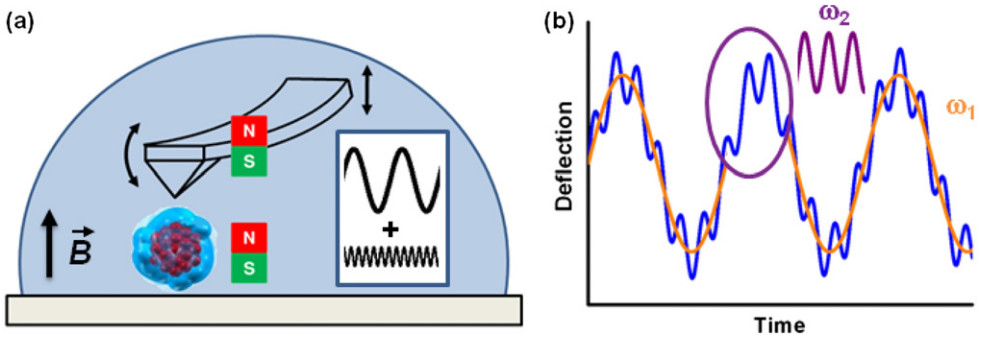

Figure 1. Scheme of bimodal AFM operation to measure simultaneously mechanical and magnetic interactions. (a) The first two cantilever–tip eigenmodes (ω_1, ω_2) are excited by applying a mechanical force at the cantilever base. Ferritin molecules are imaged in liquid in the presence of an external magnetic field. (b) The amplitude of the first mode is used to generate an image of the topography in exactly the same way as in amplitude-modulation AFM. The phase shift of the second mode ϕ_2 is used to reconstruct the structure of the protein with its mechanical (protein shell) and magnetic (iron oxide core) contributions (supporting information available at stacks.iop.org/Nano/22/125708/mmedia).

separation of forces of different natures, for example mechanical and magnetic. Imaging of magnetic structures and nanoparticles with sub-50 nm spatial resolution in air is usually accomplished with a magnetic force microscope (MFM) [11, 29, 31–33]. The fact that in MFM the tip is placed several nanometers above the surface (lift distance) implies that detecting and imaging magnetic or polarized superparamagnetic particles by magnetostatic interactions is not possible below 10–12 nm in size [11, 31–33]. Furthermore, MFM imaging of nanoparticles does not always separate electrostatic from magnetic interactions [34].

Here we develop bimodal force microscopy to simultaneously detect short-and long-range forces of different natures. The method is applied to image magnetic polarized single ferritin molecules in air and liquid with a 5 nm spatial resolution. Ferritin is a cage-shaped biomolecule that accommodates an iron oxyhydroxide nanoparticle [35]. This protein is formed by a polypeptidic hollow shell (apoferritin) that encapsulates an iron-based core that can reach a maximum diameter of 7 nm. The structure of the iron core resembles that of ferrihydrite with a nominal formula $(FeOOH)_8(FeOH_2PO_4)$.

Figure 1 shows a scheme of the bimodal AFM experiments performed in liquid on a surface containing ferritin molecules. The light blue half-sphere represents the liquid cell (figure 1(a)). Bimodal AFM involves the mechanical excitation of two cantilever eigenmodes. As a consequence of the multifrequency excitation of the cantilever, the deflection (photodiode signal) contains two dominant frequencies: $z(t) = A_1\cos(\omega_1 t - \phi_1) + A_2\cos(\omega_2 t - \phi_2) + O(\varepsilon)$ (figure 1(b)). The amplitude of the low frequency eigenmode A_1 is used to track the topography of the system while the phase shift of the high frequency component ϕ_2 contains contributions from mechanical and magnetic interactions that allow us to reconstruct the structure of the protein. The deflection might have other high-order terms $O(\varepsilon)$. However, those components are usually very small and can be neglected. Bimodal atomic force microscopy has demonstrated the ability to resolve the structure of antibodies (IgM) in air and liquid [21]. This method is also compatible with the presence of mechanical [12, 13], electrostatic [22] or magnetic interactions [25].

2. Experimental section

The bimodal excitation/detection was performed by using a custom-built electronic unit. This unit was coupled to a commercial AFM (Multimode AFM, Veeco Instruments Inc., Santa Barbara, CA, USA). The first two fundamental eigenmodes of the cantilever were excited simultaneously by the bimodal unit. We have used supersharp cantilevers (SSS-MFMR NanoAndMore GmbH, Wetzlar, Germany) coated with a thin layer of cobalt (≈25 nm). The frequencies for the first and second eigenmode of the cantilevers in air were, respectively, in the ranges of 55–65 kHz and 350–410 kHz; the spring constant for the fundamental mode determined by the Sader method [36] was $k_1 = 1.0$–1.4 N m^{-1} and the quality factor in air $Q_1 \approx 130$. The cantilever was excited to free amplitudes of $A_{01} \approx 10$ nm for the first eigenmode and $A_{02} \approx 0.5$–1.0 nm for the second eigenmode (air), and $A_{01} \approx 7$ nm and $A_{02} \approx 1$–2 nm (liquid). As a rule, the values of A_{01} are chosen to be as high as possible as operation in the attractive regime allows it to be. In order to maximize the ratio A_{01}/A_{02}, the values of A_{02} were then minimized taking into account the noise level [12]. A similar approach was followed in liquid although the values of A_{01} are smaller to avoid sample damage. The imaging ratio between the set point amplitude and the free amplitude of the first eigenmode (A/A_{01}) was about 0.9. The instrumental error in the phase shift is about 0.01°. We studied mixtures of ferritin from horse spleen (product number 96701 from Sigma Aldrich Corp. St Louis, MO, USA) and apoferritin from equine spleen (product number A3641 from Sigma Aldrich Corp., St Louis, MO, USA) or gold nanoparticles (product number: 15703-20, Ted Pella Inc., Redding, CA, USA). The molecules were deposited on mica by drop casting from a buffer solution. More details about the sample preparation and the imaging processing are found in the accompanying supporting information file (available at stacks.iop.org/Nano/22/125708/mmedia).

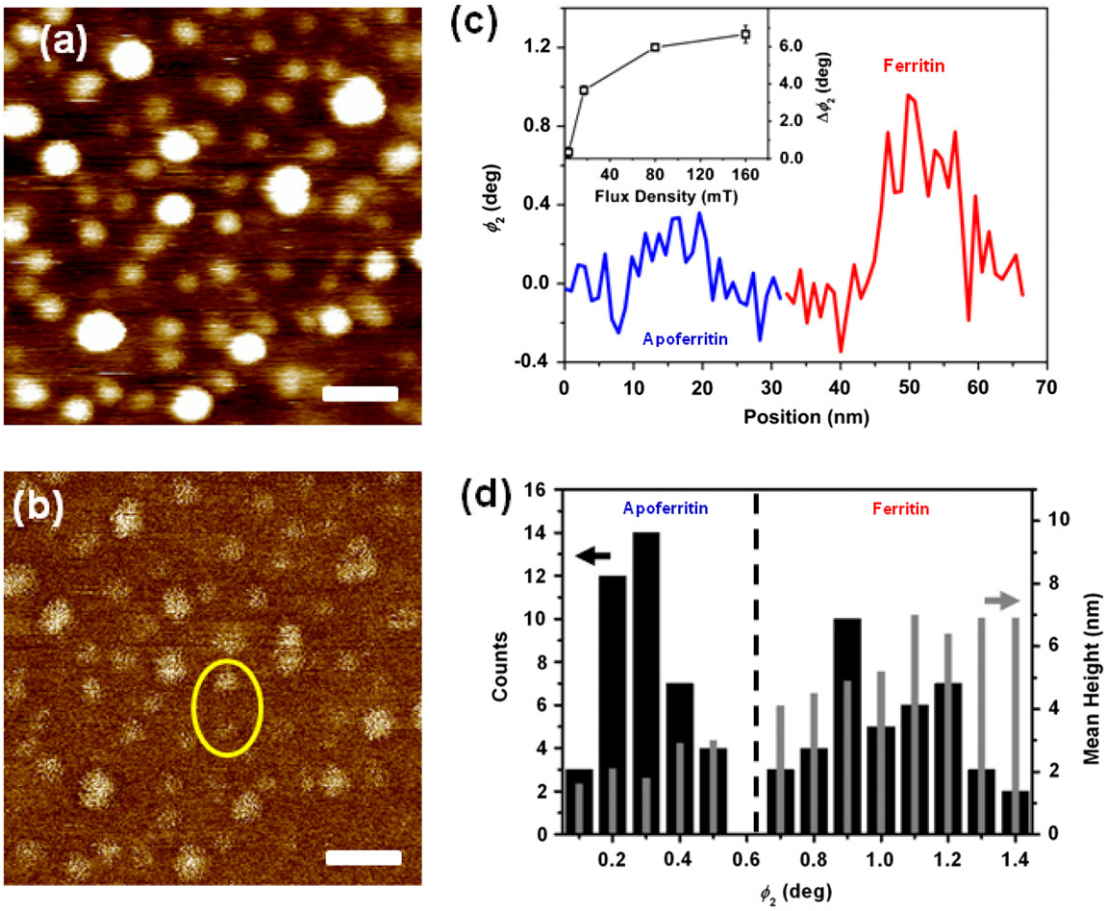

Figure 2. Topography and bimodal phase shift images in air of a deposition containing ferritin and apoferritin molecules. (a) Topography ($A_{01} = 10$ nm, $A_{sp} = 9$ nm and $A_{02} = A_2 = 0.9$ nm). (b) Bimodal phase shift image of (a). (c) Phase shift cross section of the nanoparticles marked in (a) and (b). The inset shows the average bimodal phase shift measured on ferritin with respect to the mica substrate as a function of the magnetic flux density applied to the sample. (d) Histogram of phase shift ϕ_2 (black) and mean height values (gray) of the nanoparticles. The data has been obtained from several images as the one shown in (a) and (b). Phase shift measurements range from 0.1° to 1.4°. Three main regions can be defined: $\phi_2 \in [0.1°, 0.5°]$, $\phi_2 \in [0.7°, 1.0°]$ and $\phi_2 \in [1.1°, 1.4°]$. Those regions are associated with three different type of nanoparticles: apoferritin shells, partially filled ferritin cores and saturated ferritin. The images have been acquired under the presence of a magnetic field of 80 mT. Scale bar is 50 nm.

To describe the dynamics of the cantilever–tip system we model the cantilever as a rectangular beam. The Euler–Bernoulli partial differential equation of the cantilever is approached by a system of n second-order differential equations, one for each eigenmode of the cantilever. We also assume that the dynamics of the system is mostly contained in the first two eigenmodes.

3. Results and discussion

To illustrate the ability of the technique to separate nanostructures of identical short-range mechanical properties but with different long-range interactions, we have imaged surfaces covered with a mixture of ferritin and apoferritin molecules (figure 2(a)). The measurements have been obtained under the presence of a magnetic field of 80 mT to polarize the ferritin superparamagnetic cores. The bimodal phase shift ϕ_2 cross section of the molecules marked in figure 2(b) shows significant differences (figure 2(c)). Those differences are attributed to the different types of tip–molecule interactions, either mechanical (apoferritin) or mechanical and magnetic (ferritin). We remark that the topography of the molecules marked in figure 2(b) is very similar. The inset in figure 2(c) shows the averaged bimodal phase shift of ferritin with respect to the mica substrate as a function of the magnetic flux density. The diagram shows that the bimodal phase shift increases with increasing flux density until it saturates above 150 mT. Hence, the phase shift of the second mode is dominated by the magnetic interaction between the probe and the ferritin molecules.

The histogram obtained from the bimodal phase image can be separated in three regions (figure 2(d)): $\phi_2 \in [0.1°, 0.5°]$, $\phi_2 \in [0.7°, 1.1°]$ and $\phi_2 \in [1.1°, 1.4°]$. The region with $\phi_2 < 0.5°$ concentrates 80% of the measurements at $0.3° \pm 0.1°$. Interestingly, those nanoparticles also show height values between 2 and 4 nm. We attribute those structures to apoferritin shells. In the intermediate region the nanoparticles are concentrated at $\phi_2 = 0.9° \pm 0.1°$. In this region the observed

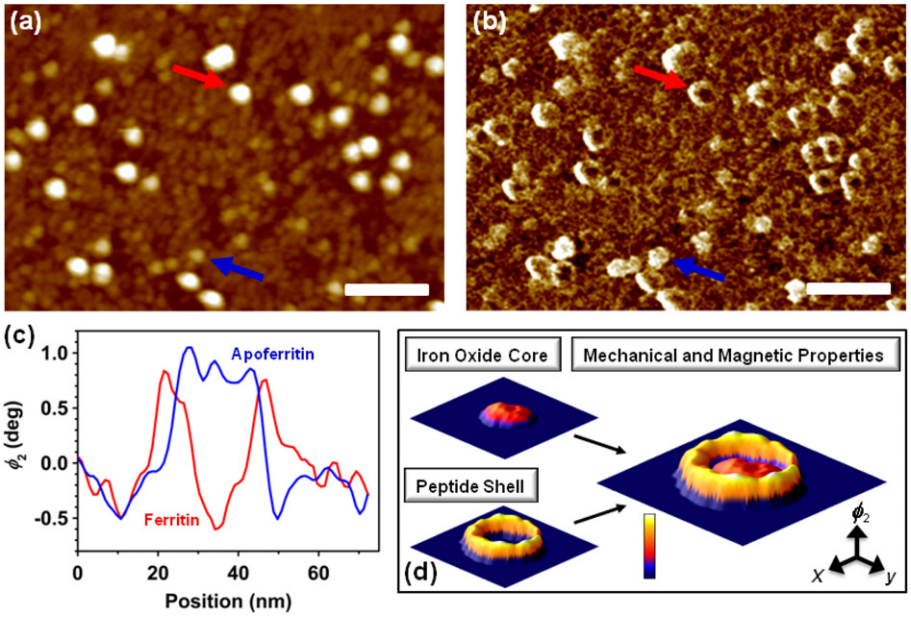

Figure 3. Topography and bimodal phase shift images in buffer (pH = 3) of a deposition containing ferritin and apoferritin molecules. (a) Topography (A_{01} = 7 nm, A_{sp} = 6 nm, A_{02} = 1.1 nm). (b) Bimodal phase shift image of (a). The phase image shows two different structures: ring-like and full nanoparticles. (c) Phase shift cross section of the nanoparticles marked in (a) and (b). (d) Bimodal phase shift image of the iron oxide core, the peptide shell and an image reconstruction of ferritin revealing the mechanical and the magnetic properties.

value of ϕ_2 increases with the height of the nanoparticle. Finally, the nanoparticles showing the largest phase shifts have an apparent height of 7 nm. The correlation observed between the phase values and height measurements is attributed to the nanoparticles made up of an apoferritin shell and an iron oxide core. In fact, we propose that the correlation observed between phase shift and height values in the intermediate region can be explained by the size of the iron oxide core. In the case of a phase shift of 0.9° we estimate a partially filled ferritin molecule with an iron core of 5 nm in diameter. Controlled experiments performed with homogeneous samples made up of either apoferritin or ferritin molecules confirm the above conclusions. The genuine magnetic contrast of the ferritin molecules has been verified by showing that the bimodal phase shift changes with the strength of the magnetic field (see the inset in figure 2(b)). Furthermore, the sign of the phase shift is reversed by inverting the polarization of the AFM probe (figures S1 and S2 available at stacks.iop.org/Nano/22/125708/mmedia).

Bimodal AFM using magnetic cantilevers is also capable to detect magnetic forces in liquid. However, the implementation of the bimodal technique in liquid is more challenging. On the one hand, the presence of the resonances of the fluid cell makes it hard to find the proper resonances of the cantilever. A thermal tuning must be carried out in order to detect the peaks corresponding to the true resonances of the cantilever. On the other hand, the change in the environment results in changes in the interaction forces. Attractive van der Waals forces are screened by the polar molecules of the liquid. As a consequence, in liquid the measurements are performed in the repulsive regime.

In figure 3 we show two images obtained in buffer (pH = 3) of a mixture of ferritin and apoferritin molecules. The topography (figure 3(a)) shows a random distribution of nanoparticles. On the other hand, the bimodal phase shift image (ϕ_2) shows two different molecules: ring-like and flat disc molecules (figures 3(b) and (c)). The ring-like structure is given by ferritin while the flat disc is given by apoferritin molecules. The phase shift cross section of the molecules (figure 3(c)) marked in figure 3(b) shows that an apoferritin molecule is characterized by a rectangular shape while a ferritin molecule is characterized by the presence of two peaks and a dip in between. This observation is in stark contrast with the bimodal AFM images obtained in air where apoferritin and ferritin showed a similar phase shift shape but the ferritin gave a stronger signal (figure 2(c)). The ring-like shape of ferritin in liquid is explained by the interplay between magnetic and mechanical interactions and the enhancement of magnetostatic interactions in the bimodal phase shift. Dynamic AFM imaging in liquid is performed under a net repulsive force. When the tip is over an apoferritin molecule, the short-range mechanical forces give rise to the topography and the bimodal phase shift images. When the tip is over a ferritin molecule, the short-range mechanical forces control the amplitude decrease as in the apoferritin case and the topography is recorded. However, the bimodal phase shift is sensitive to the presence of both short-range mechanical (repulsive) and long-range magnetic (attractive) forces. Those forces drive the bimodal phase shift in opposite directions. When the tip is on top of the ferritin the magnetic interaction is maximized and a depression in the phase shift cross section is observed (figure 3(c)). Furthermore, to validate those conclusions we have imaged a surface composed of gold (hard), ferritin (medium) and apoferritin (soft) nanoparticles in air (figures 4) and in buffer (figure S3 available at stacks.iop.org/Nano/22/125708/mmedia). Only the ferritin molecules imaged in buffer

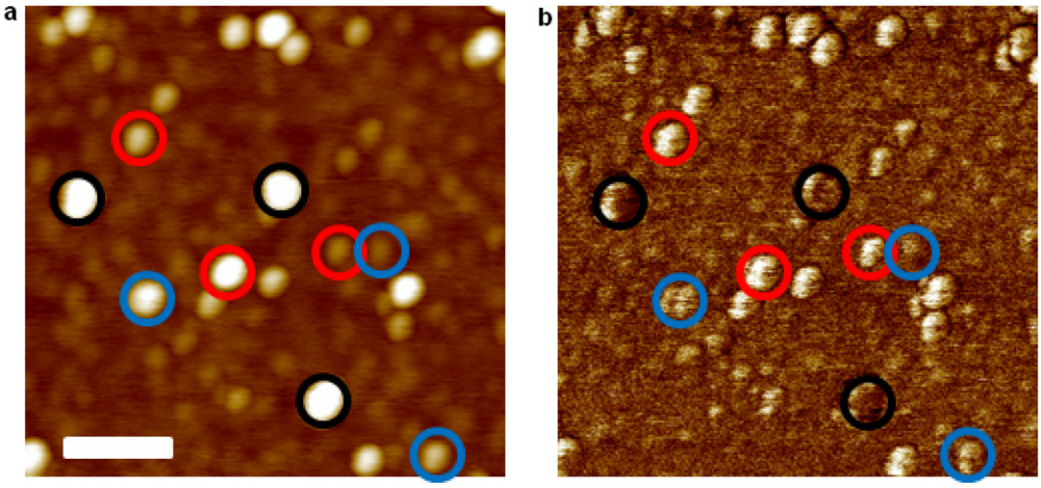

Figure 4. Mixture of ferritin, apoferritin molecules and gold nanoparticles (10 nm in diameter) deposited on mica measured in air. (a) Topography image. (b) Bimodal phase image. Ferritin, apoferritin and gold nanoparticles are circled, respectively, in red, blue and black. Apoferritin and gold nanoparticles show almost no contrast whereas ferritin appears as a bright spot due to the magnetic interaction between the molecule and the cobalt-coated cantilever. The image was measured using a cobalt-coated cantilever and by applying a magnetic flux density of 80 mT to the sample. The scale bar is 50 nm.

gave rise to ring-like structures, so the presence of a hard inorganic core is not a relevant factor in the reported contrast. As an approach for separating the short-range mechanical forces from the long-range magnetic forces we processed a high resolution bimodal phase image of a single ferritin molecule as described in detail in the supporting information (figures S4 and S5 available at stacks.iop.org/Nano/22/125708/mmedia). As a result, we obtained separate phase images for the peptide shell containing the mechanical properties and for the ferritin iron oxide core containing the magnetic properties (figure 3(d)). Variations of the bimodal phase shift within the iron oxide core lead to the conclusion that the lateral magnetic resolution of bimodal AFM in liquid is below 7 nm.

We perform a two-step theoretical study to understand the interplay among eigenmodes, mechanical and magnetic forces that give rise to the enhancement in sensitivity observed in bimodal operation. First, we discuss some analytical expressions that relate the phase shift to the gradient of the net tip–surface force in lift mode. Then, we discuss the origin of the enhanced magnetic sensitivity in bimodal AFM. By using the model of a weakly perturbed harmonic oscillator we can express the phase shift in lift mode by

$$\phi(\omega_i) = \arctan\left(\frac{\gamma\omega_i}{k_{\text{eff}} - m\omega_i^2}\right) = -\arctan\left(\frac{k_i/Q_i}{F'}\right) \quad (1)$$

with

$$k_{\text{eff}} = k_i - F' = k_i - \frac{\mathrm{d}F(z)}{\mathrm{d}z} \quad (2)$$

and

$$\gamma\omega_i = \frac{m\omega_i\omega_i}{Q_i} = \frac{k_i}{Q_i} \quad (3)$$

where $F(z)$, k_i, m, ω_i, γ and Q_i are, respectively, the total tip–surface force, the force constant, cantilever effective mass, resonant frequency, damping coefficient and quality factor of the eigenmode i.

By assuming that the force changes smoothly when the tip moves from two neighboring positions 1 and 2 of the molecule, the associated phase shift change of the ith eigenmode can be calculated as

$$\Delta\phi_i \equiv \phi_i(2) - \phi_i(1) = \frac{\partial\phi_i}{\partial F'}\Delta F' = \frac{k_i/Q_i}{F'^2 + (k_i/Q_i)^2}\Delta F' \approx \frac{Q_i}{k_i}\Delta F' \quad (4)$$

where $\Delta F' = F'(2) - F'(1)$. Thus, changes in the phase shift reflect changes in the differences of the gradient of the forces. Now, for a rectangular cantilever

$$\frac{Q_i}{k_i} = \frac{\omega_1}{\omega_i}\frac{Q_1}{k_1}. \quad (5)$$

As a consequence, under monomodal excitation/detection the compositional contrast decreases by using higher-order cantilever modes. Numerical simulations confirm the above result in the presence of slowly varying forces (quasi-linear region, figure 5(a)). However, the bimodal excitation couples the cantilever modes in the presence of nonlinear tip–surface forces. Given the difference in amplitudes ($A_1 \approx 12A_2$), the coupling modifies primarily the properties of the second mode. Thus, the phase shift of the second mode is able to detect changes in both the force and the gradient of the tip–surface forces when the tip moves from one region to the other. We relate this nonlinear effect to the increase in lateral resolution present in the second-mode phase images.

We can estimate the minimum magnetic moment detectable with bimodal AFM by assuming a simple model for fully filled and partially filled ferritin. Figure 5(b) shows the phase shift of the first eigenmode measured on ferritin molecules (average height 7 nm) with respect to the mica substrate as a function of the lift height. Applying equation (4)

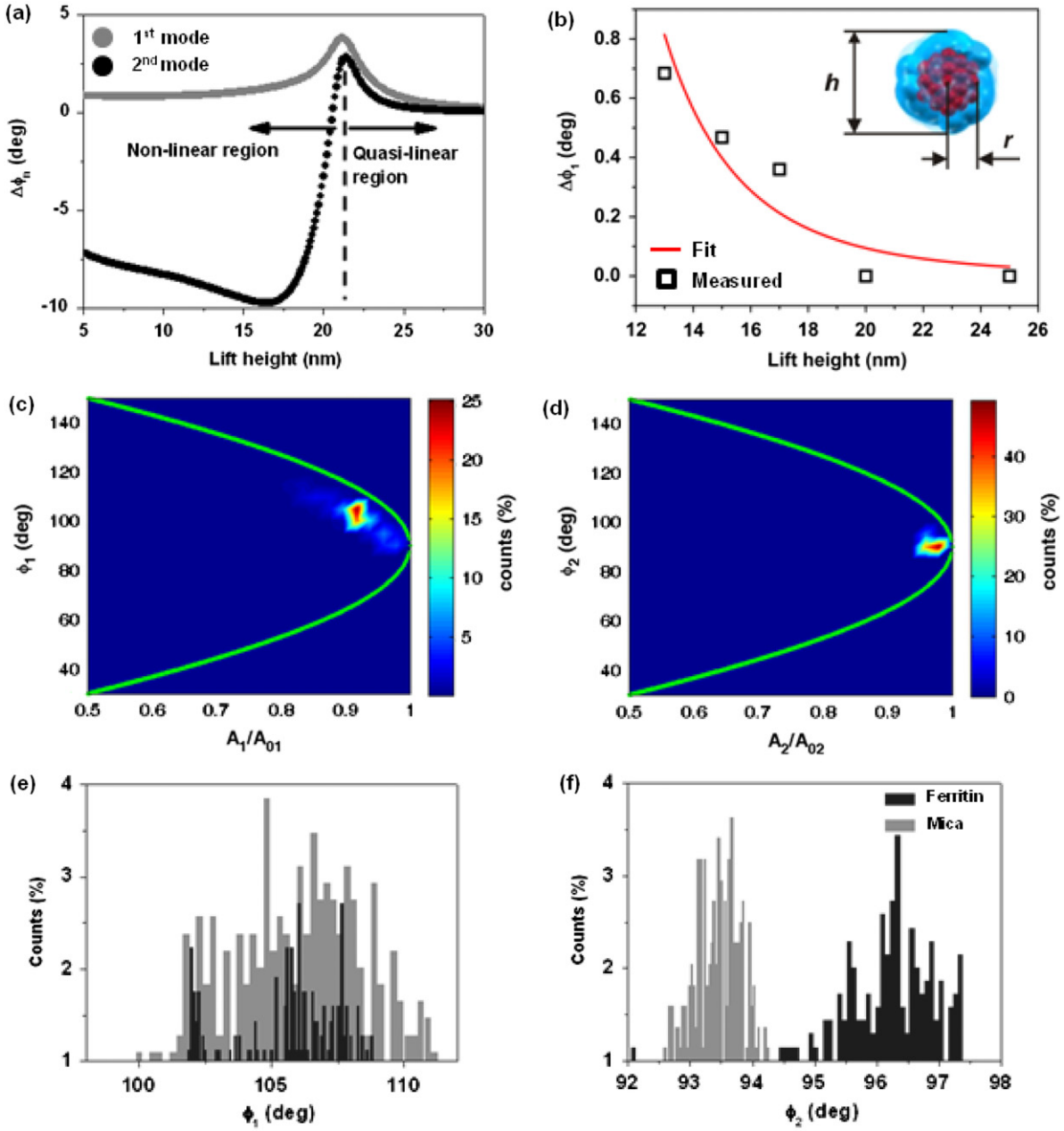

Figure 5. Phase–amplitude maps in bimodal AFM. (a) Dependence of the phase shift of eigenmodes 1 and 2 on the tip–surface distance under bimodal excitation. The phase shift of the lowest mode is more sensitive to changes in the tip–surface force in the quasi-linear region because it has a higher Q/k ratio. However, the presence of nonlinear forces enhances the sensitivity of the second mode to provide material contrast. (b) Phase shift of the first eigenmode measured on a fully filled ferritin with respect to the mica as a function of the lift height. The inset shows a sketch of a ferritin molecule with the iron core and the peptide shell. (c)–(d) Dissipation diagrams for ferritin on mica. (e) Histogram from (c) of phase shift values on mica and ferritin (first mode). (f) Histogram from (d) of phase shift values on mica and ferritin (second mode).

to the force between two magnetic dipoles yields

$$\Delta\phi_1(d) = \frac{Q_1}{k_1}F'(d) = \frac{Q_1}{k_1}\frac{\mu_0 \vec{m}_\mathrm{p}\cdot\vec{m}_\mathrm{f}}{3d^5} \qquad (6)$$

where μ_0 is the magnetic permeability of vacuum, d is the average distance between the cantilever and the sample and m_f are, respectively, the magnetic moment of the probe and the ferritin. The value of m_p is estimated as 7.1×10^5 μ_B. This value is obtained by modeling the tip apex as a magnetic sphere and using the nominal remanent magnetization of the Co coating of 80 emu cm^{-3}. By fitting the data shown in figure 5(b) to equation (6) we can extract the value for the magnetic moment of a single ferritin to be $m_\mathrm{f} \approx 200$ μ_B. In the histogram of figure 2(d) we could identify two kinds of ferritin: fully filled ferritin with an apparent height of $h_1 = 7$ nm and partially filled ferritin with an apparent mean height of $h_2 = 5$ nm. By assuming a radius of the encapsulated iron core of $r = 2$ nm (see the inset in figure 5(b)), we calculate a magnetic moment of $m'_\mathrm{f} = 50$ μ_B. This value corresponds to the minimum detectable magnetic moment in our experiments.

In order to explain the increase of the magnetic contrast provided by the second-mode phase images we have to consider how the imaging is performed. In any amplitude-modulation AFM image of a ferritin molecule, the contrast in any of the channels is related to changes in the topography, mechanical and magnetic properties of the sample. The mathematical relationships can be expressed as

$$\Delta z_{\mathrm{top}} = \Delta h + \left.\frac{\partial z_{\mathrm{c}}}{\partial H}\right|_{A_{\mathrm{sp}}} \Delta H + \left.\frac{\partial z_{\mathrm{c}}}{\partial m_{\mathrm{f}}}\right|_{A_{\mathrm{sp}}} \Delta m_{\mathrm{f}} \tag{7}$$

$$\Delta\phi_1 = \left.\frac{\partial \phi_1}{\partial H}\right|_{A_{\mathrm{sp}}} \Delta H + \left.\frac{\partial \phi_1}{\partial m_{\mathrm{f}}}\right|_{A_{\mathrm{sp}}} \Delta m_{\mathrm{f}} \tag{8}$$

$$\Delta\phi_2 = \left.\frac{\partial \phi_2}{\partial H}\right|_{A_{\mathrm{sp}}} \Delta H + \left.\frac{\partial \phi_2}{\partial m_{\mathrm{f}}}\right|_{A_{\mathrm{sp}}} \Delta m_{\mathrm{f}} \tag{9}$$

where Δz_{top} is the topography as determined by the instrument. Δh, ΔH and Δm_{f} and z_{c} are, respectively, the variations in the height, Hamaker constant, magnetization of the sample and mean tip–surface distance.

Dissipation diagrams (see supporting information available at stacks.iop.org/Nano/22/125708/mmedia) of a ferritin molecule deposited on a mica surface (air) for the first and second mode are shown, respectively, in figures 5(c) and (d). For both modes, the measured phase shift is very close to the conservative trajectory (continuous line). This indicates the conservative and non-destructive character of the tip–surface interaction. Under those conditions the contrast observed in topography and phase channels can be explained as follows. First, the contribution to Δz_{top} from changes in composition is much smaller than the changes in the true height of the sample; consequently $\Delta z_{\mathrm{top}} \approx \Delta h$. Second, the conservative nature of the interaction and constraint imposed by the feedback, which keeps the amplitude of the first mode constant, keeps the phase of the first mode at a fixed value ($\Delta\phi_1 = 0$). However, the second-mode phase channel is not affected by this constraint and shows changes in magnetic composition [37] (see equation (9)). This interpretation is in agreement with the experimental results (figure 5(e)). The histogram of the first-mode phase shows one single peak. There the contributions from the mica and the ferritin overlap. This confirms that the first mode carries no contrast between ferritin and mica. However, the histogram obtained from ϕ_2 reveals two spots (figure 5(f)). The left spot corresponds to the value obtained on the mica and the right one corresponds to the value obtained on the ferritin molecule (regions where data points were taken are indicated in figure S6 available at stacks.iop.org/Nano/22/125708/mmedia).

4. Conclusions

In conclusion, we report a nanomechanical effect that enables the identification of magnetic properties with increased lateral resolution and high magnetic sensitivity. The nanomechanical coupling between the first two cantilever modes is established by the nonlinear character of the probe–surface forces. A remarkable property of the coupling is the sensitivity to compositional changes in the presence of conservative interactions. This enables the detection of a minimum magnetic moment around 50 μ_{B} in a ferritin molecule with an estimated size of 5 nm. Moreover, we have demonstrated the application of this technique in a liquid environment with a lateral magnetic resolution below 7 nm.

Acknowledgments

We acknowledge the financial support from the Ministerio de Ciencia, Investigación e Innovación (MAT2009-08650 and CSD2010-00024).

References

[1] Maspoch D, Ruiz-Molina D, Wurst K, Domingo N, Cavallini M, Biscarini F, Tejada J, Rovira C and Veciana J 2003 *Nat. Mater.* **2** 190
[2] Cavallini M, Albonetti C and Biscarini F 2009 *Adv. Mater.* **21** 1043
[3] Pires D, Hedrick J L, De Silva A, Frommer J, Gotsmann B, Wolf H, Despont M, Duerig U and Knoll A W 2010 *Science* **328** 732
[4] Garcia R, Magerle R and Perez R 2007 *Nat. Mater.* **6** 405
[5] Raman A, Melcher J and Tung R 2008 *Nano Today* **3** 20
[6] Gan Y 2009 *Surf. Sci. Rep.* **64** 99
[7] Husale S, Persson H H J and Sahin O 2009 *Nature* **462** 1075
[8] Shekhawat G S and Dravid V P 2005 *Science* **310** 89
[9] Fukuma T, Ueda Y, Yoshioka S and Asakawa H 2010 *Phys. Rev. Lett.* **104** 016101
[10] Voïtchovsky K, Kuna J J, Contera S A, Tosatti E and Stellacci F 2010 *Nat. Nanotechnol.* **5** 401
[11] Schreiber S, Savla M, Pelekhov D V, Iscru D F, Selcu C, Hammel P C and Agarwal G 2008 *Small* **4** 270
[12] Martinez N F, Patil S, Lozano J R and Garcia R 2006 *Appl. Phys. Lett.* **89** 153115
[13] Proksch R 2006 *Appl. Phys. Lett.* **89** 113121
[14] Sahin O, Magonov S, Su C, Quate C F and Solgaard O 2007 *Nat. Nanotechnol.* **2** 507
[15] Xu X, Melcher J, Basak S, Reinferberger R and Raman A 2009 *Phys. Rev. Lett.* **102** 060801
[16] Kawai S, Glatzel T, Koch S, Such B, Baratoff A and Meyer E 2009 *Phys. Rev. Lett.* **103** 220801
[17] Hutter C, Platz D, Tholén E A, Hansson T H and Haviland D B 2010 *Phys. Rev. Lett.* **104** 050801
[18] Tetard L, Passian A and Thundat T 2010 *Nat. Nanotechnol.* **5** 105
[19] Kalinin S, Jesse S and Proksch R 2010 *R&D Mag.* **50** 20
[20] Rodriguez T R and Garcia R 2004 *Appl. Phys. Lett.* **84** 449
[21] Patil S, Martinez N F, Lozano J R and Garcia R 2007 *J. Mol. Recognit.* **20** 516
[22] Stark R W, Naujoks N and Stemmer A 2007 *Nanotechnology* **18** 065502
[23] Martinez N F, Lozano J L, Herruzo E T, Garcia F, Richter C, Sulzbach T and Garcia R 2008 *Nanotechnology* **19** 384011
[24] Dietz C, Zerson M, Riesch C, Gigler A M, Stark R W, Rehse N and Magerle R 2008 *Appl. Phys. Lett.* **92** 143107
[25] Li J W, Cleveland J P and Proksch R 2009 *Appl. Phys. Lett.* **94** 163118
[26] Yamamoto D, Taoka A, Uchihashi T, Sasaki H, Watanabe H, Ando T and Fukumori Y 2010 *Proc. Natl Acad. Sci. USA* **107** 9382
[27] Scarberry K E, Dickerson E B, McDonald J F and Zhang Z J 2008 *J. Am. Chem. Soc.* **130** 10258

[28] Huang H, Delikanli S, Zeng H, Ferkey D M and Pralle A 2010 *Nat. Nanotechnol.* **5** 602
[29] Moskalenko A V, Yarova P L, Gordeev S N and Smirnov S V 2010 *Biophys. J.* **98** 478
[30] Newman D M, Wears M L, Jollie M and Choo D 2007 *Nanotechnology* **18** 205301
[31] Hosaka S, Kikukawa A, Honda Y, Koyanagi H and Tanaka S 1992 *Japan. J. Appl. Phys.* **31** L904
[32] Schwarz A and Wiesendanger R 2008 *Nano Today* **3** 28
[33] Härtling T *et al* 2010 *Appl. Phys. Lett.* **96** 183111
[34] Neves C S, Quaresma P, Baptista P V, Carvalho P A, Araujo J P, Pereira E and Eaton P 2010 *Nanotechnology* **21** 305706
[35] Harrison P M and Arosio P 1996 *Biochim. Biophys. Acta* **1275** 161
[36] Sader J E, Chon J W M and Mulvaney P 1999 *Rev. Sci. Instrum.* **70** 3967
[37] Lozano J R and Garcia R 2008 *Phys. Rev. Lett.* **100** 076102